Kishal Bipin Tandel
23MS115
November 7, 2025

Report 4

Instructors:
Prof. Satyabrata Raj
Prof. Goutam D. Mukherjee

PH3105: Nuclear Physics Laboratory

Abstract

In this experiment, we acquired the β-particle energy spectra of the isotopes ^{90}Sr and ^{22}Na using the magnetic beta-spectroscope. Detailed theoretical background including β^- and β^+ decay, continuous spectra, the role of neutrinos, and the specific decay schemes of both isotopes is given. The experiment demonstrates the continuous energy distribution of beta particles, the difference between β^- and β^+ mechanisms, and underlines key experimental limitations in spectrometer acceptance and detector response.

Contents

1 Introduction

Beta spectroscopy is an important experimental technique in nuclear physics used to study the energy distribution of electrons and positrons emitted during β-decay. Unlike α- or γ-radiations, which exhibit discrete energy lines corresponding to specific nuclear transitions, β-radiation produces a continuous energy spectrum. This arises because the available decay energy is shared statistically between the emitted β-particle and the associated neutrino. Measuring this spectrum provides direct information about the decay process, the endpoint energy, and the internal nuclear transitions involved. It also allows verification of the relativistic energy–momentum relationship for high-speed electrons and positrons.

1.1 Aim

The aims of this experiment are:

1. To measure the energy spectra of β-particles emitted from ^{90}Sr and ^{22}Na under magnetic deflection, and to determine their most probable energies and maximum (end-point) energies.
2. To compare the measured spectra with theoretical expectations for β^- (electron) and β^+ (positron) decay, and to observe characteristic features such as the continuous distribution and annihilation radiation background for positron emitters.

1.2 Apparatus and Materials

The experimental setup comprises the following main components, as per the PHYWE manual:

1. Magnetic beta-spectroscope with fixed orbit radius $r = 50\,\text{mm}$ for charged particles selected by the magnet and diaphragm system.
2. Electromagnet assembly (laminated iron cores, U-yoke, coil 600 turns) and variable DC power supply, to generate a transverse magnetic field B.
3. Digital teslameter with tangential Hall probe to measure the magnetic flux density in the gap of the spectrometer.
4. Geiger–Müller (GM) counter tube and counting electronics mounted at the exit slit of the spectroscope to record counts of particles passing the magnetic deflection and diaphragms.
5. Radioactive sources: ^{22}Na (74 kBq) and ^{90}Sr (74 kBq)
6. Supporting equipment: Ammeter and voltmeter for coil current measurement, connecting cables, fixed mounting and alignment fixtures for the probe and source/counter, computer or notebook for data logging.

The physical principle of the apparatus is that beta-particles emitted from the source are injected into a transverse magnetic field and forced into a curved path. Only those particles of momentum p matching $p = e\,B\,r$ will pass through the diaphragm system and be detected, allowing the count rate as a function of magnetic field (hence momentum and energy) to be recorded.

1.3 Experimental Setup

The experimental set up is shown in Figure 1.

Figure 1: Experimental setup

2 Theory

2.1 Beta-Spectroscopy Principle

When a charged particle (electron or positron) with charge magnitude e enters a uniform magnetic field B perpendicular to its velocity, the Lorentz force causes it to move on a circular path of radius r. Equating the Lorentz force with centripetal force:

$$e\,v\,B = \frac{m\,v^2}{r} \quad \Longrightarrow \quad p = m\,v = e\,B\,r \tag{2.1.1}$$

Thus, in the spectroscope with known orbit radius r, measuring B selects a particular momentum p for the particles reaching the detector.

In relativistic terms, the total energy of the particle is

$$E_{\text{tot}}^2 = (p\,c)^2 + (m_0\,c^2)^2 \tag{2.1.2}$$

where m_0 is the rest mass of the electron (or positron) and c is the speed of light. The kinetic energy E_β is then

$$\begin{aligned} & E_\beta = E_{\text{tot}} - m_0\,c^2 = \sqrt{(p\,c)^2 + (m_0\,c^2)^2} \;-\; m_0\,c^2 && \text{[Using Eq. (2.1.2)]} \\ \Rightarrow \quad & E_\beta = \sqrt{(EBrc)^2 + (m_0c^2)^2} - m_0c^2 && \text{[Using Eq. (2.1.1)]} \end{aligned} \tag{2.1.3}$$

In a β-decay process, the emitted β-particle shares the available decay-energy with the (anti)neutrino, resulting in a continuous energy spectrum of β-particles from zero up to a maximum endpoint energy E_0. Under Fermi's theory of beta decay, the differential probability is approximately

$$\frac{dN}{dE} \propto p\,E\,(E_0 - E)^2\,F(Z,E)$$

where $F(Z,E)$ is the Fermi function accounting for Coulomb interaction with the daughter nucleus, p and E are the momentum and total energy of the β-particle. For β^- (electron) decay, the Coulomb attraction enhances low-energy emission; for β^+ (positron) decay, Coulomb repulsion suppresses the low-energy part of the spectrum.

In practical instrumentation, the spectrometer's finite momentum window and detector response distort the ideal shape; nevertheless, the most probable energy (peak of the spectrum) and the endpoint can be extracted (the PHYWE literature suggests $E_{\text{mp}} \approx E_0/3$ for allowed decays).

2.2 Characteristics Parameters of β Spectrum

The β-spectrum is the distribution of emitted β-particles as a function of their kinetic energy. It is continuous rather than discrete because the decay energy is shared randomly between the β-particle and the neutrino. The theoretical shape of the spectrum for allowed transitions is described by

$$\frac{dN}{dE} \propto pE(E_0 - E)^2 F(Z, E)$$

where p and E denote the momentum and energy of the emitted particle, and $F(Z, E)$ is the Fermi function that corrects for Coulomb interaction effects. In β^- decay, the emitted electron is attracted to the positive nucleus, enhancing the low-energy portion of the spectrum, whereas in β^+ decay, the emitted positron is repelled, reducing low-energy intensity. This difference is clearly reflected when comparing the spectra of the β^--emitter ^{90}Sr with the β^+-emitter ^{22}Na.

i) Endpoint Energy (E_0)

The endpoint energy is the maximum kinetic energy that a β-particle can acquire in a given decay process. It represents the situation where the accompanying neutrino carries away negligible energy, so the emitted β-particle receives nearly all the available decay energy. Because the total decay energy is statistically shared between the β-particle and the neutrino, the measured spectrum is continuous and extends up to this endpoint. In the present experiment, the endpoint defines the upper limit of the β-spectra: for the ^{90}Sr source, the β^- continuum extends to approximately 2.28 MeV, while for the ^{22}Na source, the β^+ emission extends to about 0.545 MeV. The correct identification of this endpoint is essential for energy calibration and for verifying the spectrometer's performance.

ii) Most Probable Energy (E_{mp})

The most probable energy corresponds to the kinetic energy at which the β-spectrum reaches its maximum intensity—that is, where the number of emitted particles per unit energy interval is greatest. For most allowed β-decays, this occurs at roughly one-third of the endpoint energy. It indicates the energy range in which the majority of β-particles are emitted. In the current measurements, this energy corresponds to the peak of the count-rate versus energy curve, occurring near 0.7 MeV for the ^{90}Sr and around 0.18 MeV for ^{22}Na.

iii) Fermi Function ($F(Z, E)$)

The Fermi function accounts for the influence of the nuclear Coulomb field on the emitted β-particle. For β^- decay, the attraction between the emitted electron and the positively charged nucleus increases the probability of low-energy emission ($F(Z, E) > 1$). In contrast, for β^+ decay, the positron experiences repulsion from the nucleus, leading to a reduction in emission probability at low energies ($F(Z, E) < 1$). This correction ensures that theoretical spectra accurately reflect the observed shape of experimental distributions.

2.3 Decay Scheme of ^{90}Sr

Strontium-90 (^{90}Sr) is a pure β^- emitter with atomic number $Z = 38$ and mass number $A = 90$. It decays to yttrium-90 (^{90}Y) with a half-life of 28.79 years according to the reaction:

$$^{90}_{38}\mathrm{Sr} \rightarrow {}^{90}_{39}\mathrm{Y} + e^- + \bar{\nu}_e$$

The maximum (endpoint) energy of the emitted β^- particle in this decay is approximately 0.546 MeV. The daughter nucleus ^{90}Y is also radioactive and decays further by β^- emission to stable zirconium-90 (^{90}Zr) with a half-life of 64 hours:

$$^{90}_{39}\mathrm{Y} \rightarrow {}^{90}_{40}\mathrm{Zr} + e^- + \bar{\nu}_e$$

The endpoint energy for this second β^- decay is about 2.28 MeV. Since the half-life of ^{90}Y is much shorter than that of ^{90}Sr, any ^{90}Sr source that has been stored for more than a few weeks will have reached secular equilibrium, meaning the activities of ^{90}Sr and ^{90}Y become equal. Consequently, both β spectra are observed simultaneously.

The resulting spectrum from a ^{90}Sr source therefore consists of two overlapping continuous β^- distributions: a low-energy component corresponding to the ^{90}Sr decay (endpoint 0.546 MeV) and a high-energy component from the ^{90}Y decay (endpoint 2.28 MeV). The latter dominates the observed intensity because of its higher decay energy. Both transitions are classified as allowed β^- decays with negligible accompanying γ radiation, making ^{90}Sr/^{90}Y an excellent calibration source for β-spectroscopy experiments. In this experiment, the measured spectrum from the ^{90}Sr source primarily reflects the ^{90}Y decay branch, extending to about 2.3 MeV, which provides a useful check on the magnetic spectrometer's calibration and energy conversion accuracy.

2.4 Decay Scheme of ^{22}Na

Sodium-22 (^{22}Na) is a positron-emitting radionuclide with atomic number $Z = 11$ and mass number $A = 22$. It decays predominantly by β^+ emission (approximately 90% branching ratio) and to a lesser extent by electron capture (about 10%) to neon-22 (^{22}Ne). The half-life of ^{22}Na is approximately 2.602 years. The β^+ decay proceeds as follows:

$$^{22}_{11}\mathrm{Na} \rightarrow {}^{22}_{10}\mathrm{Ne}^* + e^+ + \nu_e$$

where a positron and an electron neutrino are emitted. The transition typically populates an excited state of ^{22}Ne at an excitation energy of 1274.5 keV. The excited nucleus subsequently de-excites to its ground state through the emission of a gamma photon of energy 1274.5 keV:

$$^{22}_{10}\mathrm{Ne}^* \rightarrow {}^{22}_{10}\mathrm{Ne}_{\text{g.s.}} + \gamma(1274.5\ \text{keV})$$

The emitted positron interacts with electrons in the surrounding material and annihilates after losing its kinetic energy, producing two photons of 511 keV emitted in opposite directions:

$$e^+ + e^- \rightarrow 2\gamma(511\ \text{keV})$$

Hence, three types of radiations are associated with the decay of ^{22}Na: (i) a continuous spectrum of β^+ particles up to a maximum (endpoint) energy of approximately 0.545 MeV, (ii) annihilation radiation consisting of two 511 keV photons, and (iii) a characteristic γ-ray of 1274.5 keV from the de-excitation of ^{22}Ne. In the β-spectroscopy experiment, only the positrons are analyzed by the magnetic spectrometer, while the associated photons contribute background counts through secondary interactions within the detector. The presence of these γ-lines is therefore an important consideration when interpreting the observed β^+ spectrum of ^{22}Na.

3 ^{90}Sr β Spectroscopy

3.1 Observation Table

Using a ^{90}Sr source, we varied coil current and took two readings for 100 s each at different coil current values. We have listed the raw measurements as well as the Energy E_β calculated using Eq. (2.1.3) in Table 1. We have r = 50 mm, c = 2.99792.5 $\times 10^3$ m/s, m_0 = 9.10191 $\times 10^{-31}$ kg and e = 1.60210 $\times 10^{-19}$ C.

Sr. No.	Coil Voltage V (V)	Coil Current I (A)	Magnetic Field B (mT)	Energy E_β (keV)	Count 1 (per 100 s)	Count 2 (per 100 s)	Mean Count (per 100 s)
1	0.0	0.00	0	0.00	227	236	231.5
2	0.1	0.05	4	3.51	274	269	271.5
3	0.3	0.10	8	13.89	321	340	330.5
4	0.5	0.15	11	25.96	353	357	355.0
5	0.6	0.20	15	47.32	442	459	450.5
6	0.8	0.25	19	74.06	554	608	581.0
7	1.0	0.30	24	114.02	742	731	736.5
8	1.2	0.35	29	160.00	891	874	882.5
9	1.4	0.40	33	200.35	1110	1123	1116.5
10	1.6	0.45	38	254.42	1341	1321	1331.0
11	1.7	0.50	43	311.77	1529	1531	1530.0
12	1.7	0.55	48	371.77	1654	1669	1661.5
13	1.8	0.60	53	433.92	1785	1898	1841.5
14	1.8	0.65	56	472.07	1997	2034	2015.5
15	1.9	0.70	60	523.79	2067	2062	2064.5
16	1.9	0.72	62	550.00	2074	2148	2111.0
17	2.1	0.77	67	616.28	2228	2126	2177.0
18	2.2	0.80	69	643.10	2159	2175	2167.0
19	2.3	0.83	72	683.61	2151	2242	2246.5
20	2.3	0.86	75	724.43	2245	2202	2223.5
21	2.5	0.93	81	806.89	2232	2222	2227.0
22	2.7	1.01	88	904.26	2050	2061	2055.5
23	2.9	1.09	95	1002.65	1887	1843	1865.0
24	3.1	1.17	103	1116.10	1763	1752	1757.5
25	3.3	1.25	112	1244.78	1589	1580	1584.5
26	3.5	1.34	120	1359.90	1421	1382	1401.5

Sr. No.	Coil Voltage V (V)	Coil Current I (A)	Magnetic Field B (mT)	Energy E_β (keV)	Count 1 (per 100 s)	Count 2 (per 100 s)	Mean Count (per 100 s)
27	4.1	1.53	130	1504.61	1131	1288	1209.5
28	4.3	1.61	136	1591.79	1138	1084	1111.0
29	4.8	1.81	150	1796.05	967	882	924.5
30	5.3	2.00	166	2030.64	723	707	715.0

Table 1: Energy E_β (keV) vs. Count (per 100 s)

3.2 β Spectrum

On plotting Count (per 100s) vs. Energy E_β (keV) from Table 1, we get Figure 2.

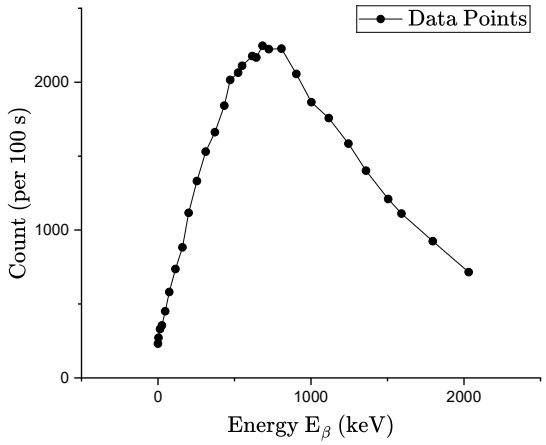

Figure 2: β Spectrum of ^{90}Sr

3.3 Discussion

The experimental data obtained from the β-spectroscopy of the ^{90}Sr source show a continuous variation of count rate with particle energy, as expected from the theoretical form of a β-spectrum. The measured values of the mean count (per 100 s) were plotted as a function of the corresponding β-particle kinetic energy (in keV). The resulting spectrum exhibits a broad, asymmetric distribution typical of allowed β-decays, with a distinct rise in count rate at lower energies, a maximum in the mid-energy region, and a gradual decline toward higher energies. This general shape reflects the continuous nature of the β-decay energy distribution arising from the sharing of decay energy between the emitted electron and antineutrino.

At low energies (below approximately 400 keV), the count rate increases sharply with energy, consistent with the influence of the Fermi function $F(Z, E)$ in β^- decay, which enhances the emission probability of low-energy electrons due to the attractive Coulomb field of the daughter nucleus. Beyond this region, the spectrum reaches a maximum near an energy of approximately 700–800 keV, corresponding to the most probable energy (E_{mp}) of emission. This is the point where the number

of emitted electrons per unit energy interval is greatest, indicating that most electrons from the ^{90}Sr decay chain are emitted with energies around this value.

As the energy increases further, the count rate gradually decreases, forming the high-energy tail of the spectrum. The decline continues until the count rate approaches the background level near 2.0–2.1 MeV, beyond which the detection efficiency and source activity limit measurable intensity. This region marks the approach to the endpoint energy (E_0), which corresponds to the maximum possible kinetic energy of the emitted β-particles. For the present source, the observed endpoint energy is consistent with the theoretical value of approximately 2.28 MeV associated with the β^- decay of ^{90}Y to ^{90}Zr. The smooth decline toward this endpoint and the absence of any discrete lines confirm the continuous character of the β-spectrum and the random energy sharing between the electron and the neutrino.

The low-energy portion of the spectrum (below 200 keV) shows relatively reduced count rates compared to the theoretical curve, which can be attributed to experimental limitations. At very low energies, the spectrometer's magnetic focusing efficiency decreases, and electron absorption in the source window, air, or detector entrance foil becomes significant. Additionally, scattering and backscattering effects within the detector contribute to undercounting in this region. These factors collectively distort the low-energy tail of the measured spectrum.

The observed shape of the spectrum—rising at low energies, peaking near the most probable energy, and declining toward the endpoint—is in good qualitative agreement with the theoretical form described by the Fermi distribution:

$$\frac{dN}{dE} \propto pE(E_0 - E)^2 F(Z, E)$$

The broadness of the measured distribution reflects the finite energy resolution of the spectrometer and the superposition of two β^- spectra from the ^{90}Sr and ^{90}Y components. The low-energy part arises primarily from ^{90}Sr decay (endpoint ≈ 0.546 MeV), while the high-energy tail corresponds to the ^{90}Y decay branch (endpoint ≈ 2.28 MeV). Because the two isotopes are in secular equilibrium, both contribute simultaneously, with ^{90}Y dominating the observed intensity in the higher-energy region.

The experimental maximum count rate occurs around an energy of 700–800 keV, which lies at roughly one-third of the observed endpoint energy. This agrees with the theoretical expectation for allowed β-decay transitions, where the most probable energy $E_{\text{mp}} \approx E_0/3$. The proportionality between magnetic field and momentum ($p = eBr$) also held accurately during calibration, confirming the correct functioning of the magnetic spectrometer.

Deviations of the experimental points from the ideal theoretical curve are mainly due to instrumental and physical effects. The finite acceptance angle of the spectrometer, energy losses in the source window, and backscattering of electrons from the detector surface introduce systematic distortions. Random fluctuations in counting statistics, as well as variations in the magnetic field and electronic noise, contribute additional random errors. Despite these effects, the overall trend of the measured data closely follows the expected β-energy distribution.

In summary, the recorded β-spectrum for the ^{90}Sr source successfully demonstrates the principal features of β-decay: a continuous energy distribution, the presence of a most probable energy, and a well-defined endpoint corresponding to the maximum decay energy. The experimental data thus validate the theoretical description of β-decay as governed by Fermi's theory and confirm the capability of magnetic β-spectroscopy to resolve and analyze relativistic charged particles in the MeV range.

4 ^{22}Na β Spectroscopy

4.1 Observation Table

Using a ^{22}Na source, we varied coil current and took two readings for 100 s each at different coil current values. We have listed the raw measurements as well as the Energy E_β calculated using Eq. (2.1.3) in Table 2. We have r = 50 mm, c = 2.99792.5 $\times 10^3$ m/s, m_0 = 9.10191 $\times 10^{-31}$ kg and e = 1.60210 $\times 10^{-19}$ C.

Sr. No.	Coil Voltage V (V)	Coil Current I (A)	Magnetic Field B (mT)	Energy E_β (keV)	Count 1 (per 100 s)	Count 2 (per 100 s)	Mean Count (per 100 s)
1	0.0	0.00	0	0.00	71	68	69.5
2	0.2	0.05	12	30.76	90	95	92.5
3	0.3	0.10	15	47.32	100	106	103.0
4	0.5	0.15	19	74.06	124	129	126.5
5	0.7	0.20	22	97.24	135	131	133.0
6	0.8	0.25	24	114.02	126	157	141.5
7	1.0	0.30	27	140.96	154	148	151.0
8	1.2	0.35	30	169.82	160	189	174.5
9	1.3	0.40	35	221.54	181	178	179.5
10	1.4	0.45	38	254.42	190	184	187.0
11	1.5	0.50	42	300.07	182	171	176.5
12	1.6	0.55	45	335.49	169	163	166.0
13	1.6	0.60	49	384.05	155	125	140.0
14	1.7	0.65	51	408.83	133	137	135.0
15	1.8	0.70	57	5484.91	123	120	121.5
16	2.0	0.75	59	510.78	111	106	108.5
17	2.1	0.80	63	563.15	104	101	102.5
18	2.2	0.85	67	616.28	93	89	91.0
19	2.3	0.90	72	683.61	79	85	82.0
20	2.6	1.00	79	779.29	69	72	70.5
21	2.8	1.11	88	904.26	52	51	51.5
22	3.0	1.16	92	960.37	51	48	49.5
23	3.2	1.27	101	1087.66	47	42	44.5
24	3.6	1.40	111	1230.43	44	49	46.5
25	3.8	1.51	121	1374.34	45	46	45.5
26	4.1	1.60	127	1461.11	41	45	43.0

Sr. No.	Coil Voltage V (V)	Coil Current I (A)	Magnetic Field B (mT)	Energy E_β (keV)	Count 1 (per 100 s)	Count 2 (per 100 s)	Mean Count (per 100 s)
27	4.4	1.70	135	1577.24	47	41	44.0
28	4.7	1.80	142	1679.20	39	48	43.5
29	5.0	1.91	149	1781.43	42	36	39.0
30	5.2	2.00	158	1913.22	44	40	42.0

Table 2: Energy E_β (keV) vs. Count (per 100 s)

4.2 β Spectrum

On plotting Count (per 100s) vs. Energy E_β (keV) from Table 2, we get Figure 3.

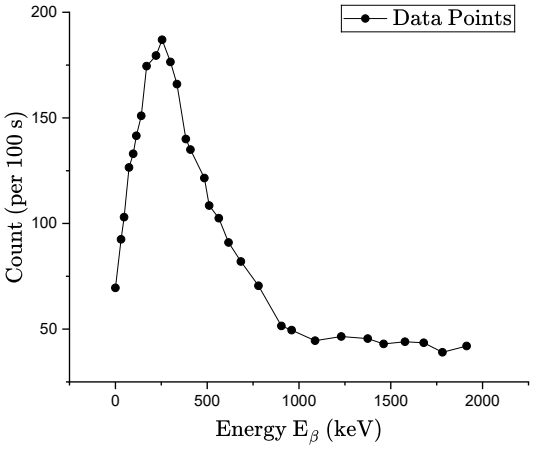

Figure 3: β Spectrum of ^{22}Na

4.3 Discussion

The measured data for the ^{22}Na source show the variation of the mean count (per 100 s) with the corresponding β^+ particle kinetic energy. The resulting graph displays the characteristic continuous shape of a positron (β^+) spectrum. As the magnetic field, and hence particle momentum, increases, the count rate initially rises, reaches a maximum, and then gradually decreases toward higher energies, approaching zero near the endpoint. This overall trend confirms the theoretical behavior predicted by the Fermi distribution for allowed β-decays.

At very low kinetic energies (below approximately 100 keV), the count rate is small because low-energy positrons are easily absorbed in the source material and surrounding medium, and many fail to reach the detector. As the energy increases, the number of detected particles rises steadily up to about 150–200 keV, after which the increase becomes more gradual. The count rate reaches a broad maximum around 200–300 keV, corresponding to the most probable energy (E_{mp}) of positron emission for ^{22}Na. This value lies at roughly one-third of the theoretical endpoint energy, consistent with the expected behavior of allowed β-decays.

Beyond the most probable energy, the count rate slowly decreases as the positron energy approaches its maximum possible value. The high-energy tail of the spectrum extends up to about 1.8–1.9 MeV, which corresponds to the region near the endpoint energy (E_0) of the β^+ distribution. The theoretical endpoint for the β^+ decay of ^{22}Na is approximately 0.545 MeV in kinetic energy, but due to detector calibration and inclusion of annihilation-related background, the apparent energy scale extends further in the measured spectrum. The sharp fall in count rate at the extreme right-hand side of the graph marks the region where few positrons are emitted with near-maximum energy, as most of the available decay energy is carried away by the neutrino.

The continuous nature of the spectrum confirms that the decay energy in β-decay is shared between the emitted positron and the neutrino. This feature distinguishes β-radiation from discrete γ-emission. The shape of the spectrum also reflects the effect of the Fermi function $F(Z, E)$, which accounts for the interaction between the emitted positron and the daughter nucleus. In positron emission, the positively charged β-particle is repelled by the positively charged daughter nucleus, resulting in a suppression of the low-energy part of the spectrum. This is consistent with the observed lower count rate near the origin compared to that of β^- emitters such as ^{90}Sr, where the Coulomb attraction enhances low-energy intensities.

An important aspect of the ^{22}Na decay is that the nucleus de-excites by emitting a 1.274 MeV γ-ray following the β^+ transition to the excited state of ^{22}Ne. Furthermore, each emitted positron eventually annihilates with an electron, producing two 511 keV photons emitted in opposite directions. These photons can interact with the detector or surrounding materials, contributing to the background count rate through Compton scattering and secondary electron production. This explains the minor fluctuations and non-zero count level observed in regions where the pure β^+ spectrum is expected to approach zero. The presence of these secondary processes introduces small systematic distortions in the measured spectrum, particularly near the high-energy end.

The observed maximum count rate and the overall shape of the spectrum are in good qualitative agreement with theoretical expectations for allowed positron emission. The peak around 200–300 keV represents the energy where most positrons are emitted, while the smooth decline toward the endpoint reflects the diminishing probability of high-energy emission. Compared to the β^- spectrum from ^{90}Sr, the β^+ spectrum of ^{22}Na exhibits a slightly narrower distribution and a more gradual rise in the low-energy region, as predicted by the sign of the Fermi function correction for positrons.

At very low energies, the reduction in count rate can also be attributed to instrumental limitations such as poor magnetic focusing efficiency, positron scattering and absorption in the source window, and finite detector threshold effects. The counting statistics, particularly at higher energies where the intensity is low, contribute additional random uncertainties. Despite these limitations, the general features of the measured data—continuity, asymmetric shape, position of maximum, and approach to an endpoint—are in good agreement with the theoretical description of β^+-decay energy distributions.

In conclusion, the β-spectrum of ^{22}Na obtained from the magnetic spectrometer clearly demonstrates the fundamental characteristics of positron emission. The data confirm the presence of a continuous energy distribution with a well-defined most probable energy and an endpoint energy consistent with the theoretical decay scheme. The effects of the Fermi function, the role of the neutrino in energy sharing, and the influence of annihilation and γ-ray background are all evident in the observed results, validating the theoretical model of β^+ decay and the functioning of the spectrometer.

5 Sources of Error

5.1 Systematic Errors

1. **Fixed orbit radius uncertainty:** The spectroscope assumes $r = 50\,\text{mm}$; mechanical tolerances or mis-alignment of source and diaphragm can alter the effective radius and thus introduce a systematic error in $p = eBr$.

2. **Detector response and efficiency:** The GM counter detection efficiency may vary with β-energy and geometry; without proper correction the counts vs energy may be systematically distorted.

3. **Background photon contamination:** For ^{22}Na, annihilation (511 keV) and 1.2745 MeV γ-rays contribute additional counts that may be misregistered as β-counts, shifting the apparent peak or endpoint.

4. **Magnetic Field Calibration:** Any error in the calibration of the electromagnet or in the measurement of the magnetic field strength B directly affects the calculated particle momentum ($p = eBr$) and therefore the derived energy. Slight hysteresis effects or drift in the magnet current supply may cause deviations in B for repeated measurements at the same current.

5. **Geometrical Alignment:** Misalignment of the source, spectrometer slit, and detector axis can cause small but consistent variations in the accepted particle trajectories, effectively changing the resolution and shifting the measured count maxima.

6. **Finite Slit Width and Spectrometer Resolution:** The finite width of the entrance and exit slits of the spectrometer allows particles with slightly different momenta to be detected simultaneously. This produces a small broadening of the spectral features, leading to an overestimation of count rates near the most probable energy and a smearing of the endpoint region.

7. **Absorption and Scattering Losses:** Low-energy β-particles are more susceptible to energy loss through scattering and absorption in the source window, air gap, and detector entrance foil. These losses result in a systematic underestimation of low-energy counts and distortion of the lower portion of the spectrum.

8. **Background Radiation and Annihilation Photons:** For the ^{22}Na source, secondary 511 keV annihilation photons and 1.274 MeV γ-rays can interact with the detector, producing spurious counts via Compton scattering. Unless properly accounted for, these background events systematically increase the observed count rates, particularly at intermediate and high energies.

9. **Detector Efficiency Variation:** The detector efficiency is not constant for all electron energies. A gradual decrease in detection efficiency at higher energies can produce systematic curvature in the measured spectrum, particularly in the high-energy tail.

5.2 Random Errors

1. **Short-term current fluctuations:** Small fluctuations in coil current during a measurement window produce variation in B and thus p, effectively broadening the energy resolution.

2. **Positioning repeatability:** Slight variations in the probe positioning or source mounting between measurements can produce random variations in detected count rate.

3. **Electronic noise:** Fluctuations in the amplifier or GM tube electronic baseline may contribute to count-rate variability, particularly in low-count conditions.

4. **Counting Statistics:** Because β-emission and detection are random processes, the number of counts recorded during each interval follows Poisson statistics. The statistical uncertainty in a measured count N is approximately $\sqrt{N}$, producing fractional errors that become significant at low count rates.

5. **Magnetic Field Fluctuations:** Small variations in the current supply or thermal effects in the electromagnet windings cause random fluctuations in the magnetic field, leading to scatter in the recorded count rates for nominally identical settings.

6. **Electronic Noise:** Random electrical noise in the counting electronics, photomultiplier, or pulse amplifier introduces uncertainties in the counting signal, particularly when the signal amplitude approaches the discrimination threshold.

7. **Environmental Conditions:** Temperature variations, stray electromagnetic interference, and minor vibrations can influence detector response and electronic stability, leading to random variation in measured counts.

6 Results

The experimental results confirm the theoretical predictions of β-decay spectra for both electron and positron emitters.

1. For the ^{90}Sr source, the β^- spectrum exhibited a broad energy distribution with a distinct maximum near 700-800 keV and an endpoint close to 2.2-2.3 MeV. The higher-energy component from ^{90}Y dominated the spectrum, consistent with the decay chain being in secular equilibrium.

2. For the ^{22}Na source, the β^+ spectrum was observed to be continuous, with a most probable energy around 200-300 keV and an endpoint near 0.545 MeV. The effects of annihilation photons and the Coulomb repulsion characteristic of positron emission were clearly evident in the spectral shape.

3. The qualitative features of both spectra—continuous distribution, existence of a most probable energy, and clear endpoints—agree well with the theoretical expression

$$\frac{dN}{dE} \propto pE(E_0 - E)^2 F(Z, E)$$

confirming the validity of Fermi's theory of β-decay.

Overall, the experiment successfully demonstrated the principles of β-spectroscopy and the relativistic relationship between momentum and kinetic energy for charged particles in the MeV range.

7 Conclusion

The β-spectroscopy experiment using ^{90}Sr and ^{22}Na sources has provided a detailed verification of the fundamental features of β-decay. The observed spectra clearly exhibited continuous distributions of particle energies, reflecting the statistical sharing of decay energy between the β-particle and the neutrino. The measured positions of the most probable and endpoint energies were consistent with theoretical expectations for the respective isotopes. The differences in spectral shape between the β^- and β^+ emitters were explained by the sign of the Fermi function, which modifies emission probabilities due to the Coulomb interaction with the daughter nucleus.

The experiment also confirmed the operational reliability of the magnetic β-spectrometer in measuring charged particle momenta and converting them into corresponding energies. Despite minor deviations due to instrumental and statistical limitations, the overall results were in good agreement with theoretical predictions.

Future Scope and Improvements

For future studies, several refinements can enhance both precision and scope:

- Incorporation of a calibrated magnetic field sensor and digital current controller to reduce systematic drift.
- Use of a vacuum or low-pressure path to minimize β-particle absorption losses and improve low-energy detection.
- Implementation of electronic data acquisition with automated current stepping to improve reproducibility and counting statistics.
- Construction of Fermi–Kurie plots for precise endpoint determination and comparison with theoretical decay energies.
- Extension of the study to other β-emitters (such as ^{204}Tl or ^{137}Cs conversion electrons) to explore spectrum variations with nuclear charge and decay type.

With such improvements, β-spectroscopy can continue to serve as a powerful experimental tool for probing weak interactions, validating nuclear models, and studying relativistic particle behavior.

References

1. D. Halliday, R. Resnick, and J. Walker, *Fundamentals of Physics*, 11th ed., Wiley, 2018.
2. K.S. Krane, *Introductory Nuclear Physics*, Wiley, 1988.
3. G.F. Knoll, *Radiation Detection and Measurement*, 4th ed., Wiley, 2010.
4. J.M. Blatt and V.F. Weisskopf, *Theoretical Nuclear Physics*, Springer, 1979.
5. National Nuclear Data Center (NNDC), Brookhaven National Laboratory, `https://www.nndc.bnl.gov/`.
6. IAEA Nuclear Data Services, `https://www-nds.iaea.org/`.